Local measurements in turbulence flows

New Challenges in Turbulence Research V, Les Houches

April, 12^{th}, 2019

Examples of local probes

- Hot wire (CTA)
- Cantilever anemometers

Frozen turbulence

- Local Taylor hypothesis
- Elliptic approximation

Experimental characterisation of turbulence

- Longitudinal velocity increments
- Application: energy cascade in superfluid flows
- Extended Self-similarity
- Application: intermittency of superfluid flows

Outline

Examples of local probes

- Hot wire (CTA)
- Cantilever anemometers

Frozen turbulence

- Local Taylor hypothesis
- Elliptic approximation

Experimental characterisation of turbulence

- Longitudinal velocity increments
- Application: energy cascade in superfluid flows
- Extended Self-similarity
- Application: intermittency of superfluid flows

Hot-wire anemometry

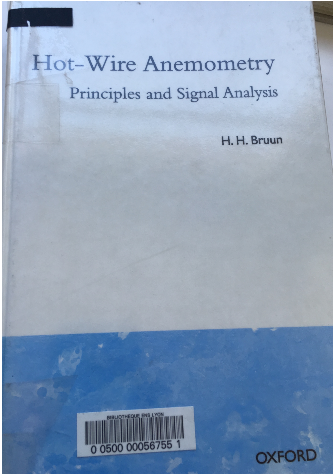

Principe of constant temperature hot-wire anemometer

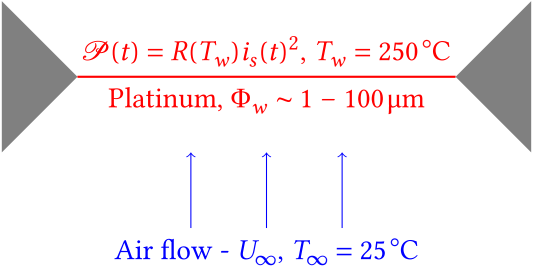

XII. *On the Convection of Heat from Small Cylinders in a Stream of Fluid: Determination of the Convection Constants of Small Platinum Wires with Applications to Hot-Wire Anemometry.*

By LOUIS VESSOT KING, *B.A.* (*Cantab.*), *Assistant Professor of Physics McGill University, Montreal.*

Communicated by Prof. HOWARD T. BARNES, *F.R.S.*

Received May 5,—Read May 28, 1914.

Thermal convection around the wire element

- Fluid property

$$Pr = \frac{\nu}{\kappa} \tag{1}$$

- Driving

$$Re = \frac{\Phi_w U_\infty}{\nu} \tag{2}$$

$$Gr = \frac{g\alpha(T_w - T_\infty)\Phi_w^3}{\nu^2} \tag{3}$$

- Response

$$Nu = \frac{\mathscr{P}\Phi_w}{\lambda S(T_w - T_\infty)} \tag{4}$$

Thermal convection around the wire element

- Dimensional analysis

$$Nu = f(Re, Gr, Pr, T_w/T_\infty) \tag{5}$$

- Two practical cases:
  - Free convection (low velocity)

$$Nu = f(Gr, T_w/T_\infty) \tag{6}$$

  - Forced convection (high velocity)

$$Nu = f(Re, T_w/T_\infty) \tag{7}$$

L. V. King, Phil. Trans. R. Soc. London, Ser. A, **214** (1914)

- Theoretical analysis for infinite wire within Boussinesq conditions,

$$\mathscr{P} = A\sqrt{U} + B \tag{8}$$

i.e. in non-dimensional terms,

$$Nu = \alpha Re^{1/2} + \beta \tag{9}$$

where α and β may depend on T_w/T_∞ and Φ_w.

L. V. King, Phil. Trans. R. Soc. London, Ser. A, **214** (1914)

- Experimental analysis

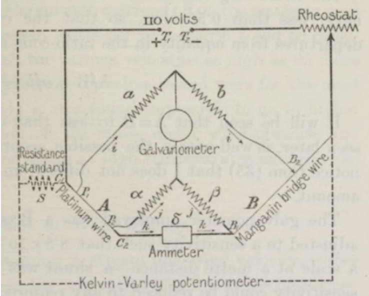

Fig. 2. Kelvin bridge connections.

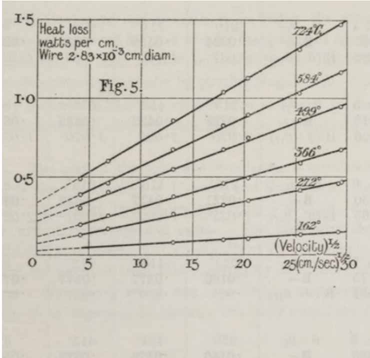

Fig. 5. *Heat-Loss Velocity Curves. Wire No. 10.*

Corrections to King model: Collis & Williams (1959)

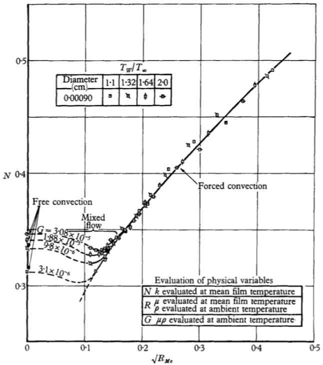

FIGURE 8. Interaction of free and forced convection.

- Buoyancy effects are small provided

$$Re > Gr^{1/3} \text{ for } Re > 0.1 \qquad (10)$$

$$Re > 1.85 Gr^{0.39} \left(\frac{T_m}{T_\infty}\right)^{0.76} \quad \text{for } Re < 0.1 \qquad (11)$$

- Yields a minimum velocity, V_{min} which can be measured without ambiguity by a hot wire
- Buoyancy effects quickly negligible when $V > V_{min}$.

Corrections to King model: Collis & Williams (1959)

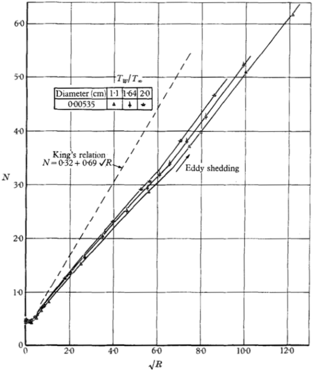

FIGURE 5. Demonstration of the inadequacy of the heat transfer relation $N = A + B\sqrt{R}$.

- Empirical relation

$$Nu\left(\frac{T_m}{T_\infty}\right)^{-0.17} = A + BRe^n \quad (12)$$

	$0.02 < Re < 44$	$44 < Re < 140$
n	0.45	0.51
A	0.24	0
B	0.56	0.48

Example of TSI 1201 hot-film with CTA-1750 anemometer

Wire length	3.2 mm
Wire diameter	50.8 µm
Wire temperature	250 °C
Air temperature	25 °C
Re_c	0.16
V_{min}	4.9 cm/s

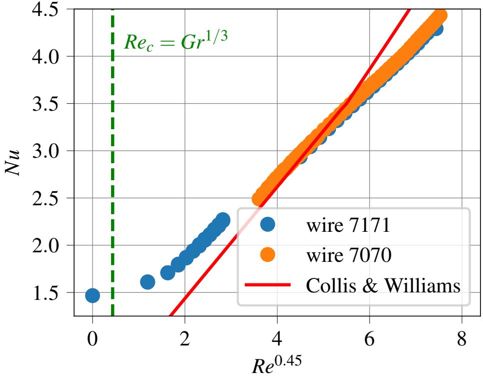

Data from Kenza Ya internship (IUT Saint-Étienne)

Alternative design

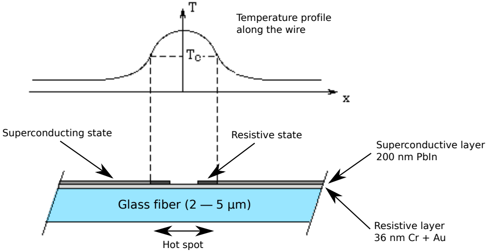

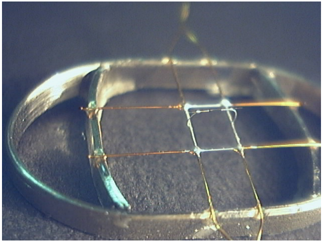

Castaing, Chabaud, Hébral, Rev. Sci. Instrum. (1992)

PbIn hot-wire:

- Microfabrication techniques
- Low thermal capacity at low temperature: **fast response** Up to ~ MHz dynamics
- Hot-spot: $\sim 17 - 20\mu m$
- More than 4 decades of resolved inertial regime

Original GReC experiment Pietropinto, *et al.*, Physica C (2003)

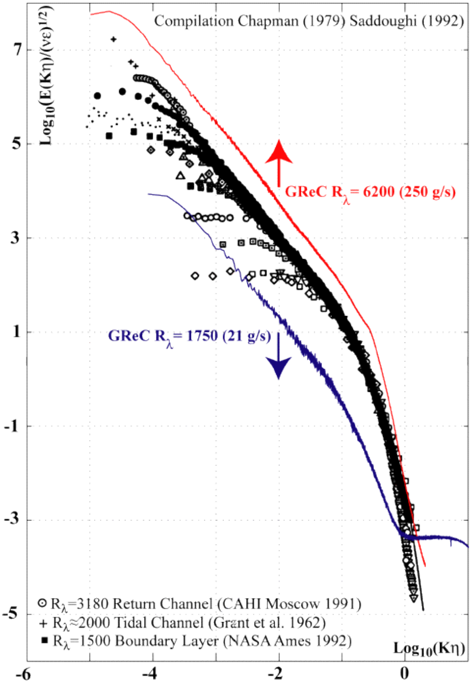

Resistive low-temperature hot-wire

- Superconductor based: very sensitive but sometimes unstable
- Lot of work to improve the spatial resolution
- Another technology: Au-Ge based

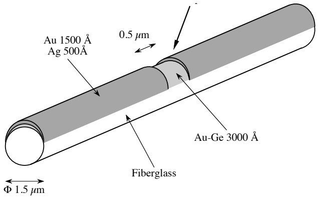

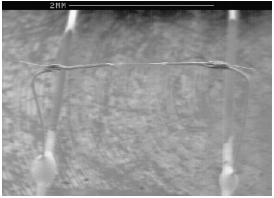

Chanal, *et al.*, Rev. Sci. Instrum. (1997)

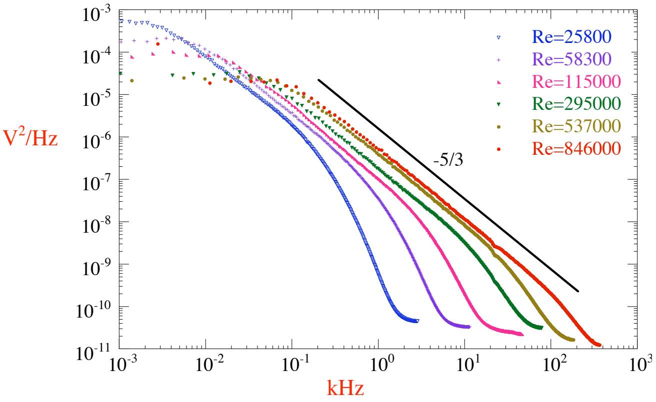

Dynamics: > 200 kHz (CTA electronics limited)

Effective spatial resolution: $\sim 6\ \mu$m

Chanal, *et al.*, Eur. Phys. J. B (2000)

Carbon fiber based hot-wires

Systematic cryogenic tests of carbon fibers were done by B. Chabaud

Carbon fiber based hot-wires

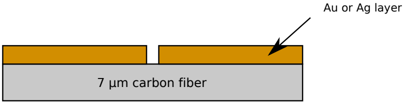

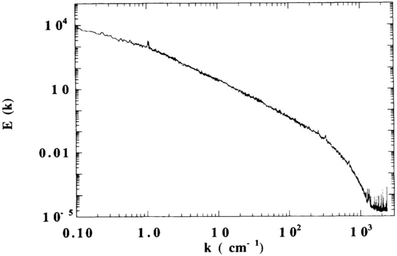

Power density spectrum of the velocity fluctuations, at 908 mbar in a Von Kármán flow with a rotation frequency of 20 Hz. $R_\lambda = 1900$.

J. Maurer, *et al.*, EPL (1994)
F. Moisy, *et al.*, PRL (1999)

Princeton Nanoscale thermal anemometry probe (NSTAP)

30 or 60 × 1 × 0.1 μm platinum filament

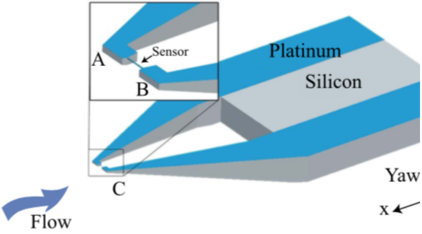

Fig. 1. 3D model of the Nano-Scale Thermal Anemomet

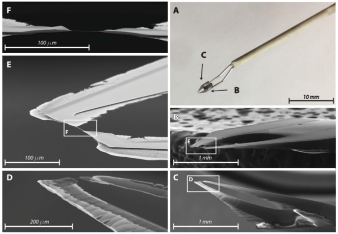

Fig. 6. A photo and Environmental Scanning Electron Microscope images of a 30 μm NSTAP. A) Probe mounted onto prongs (photo). B) Full sensor from above; C) Full sensor from below; D) Close view of the sensor from below; E) Close view of the sensor from above; F) Zoom-in on the freestanding wire.

Vallikivi & Smits, IEEE Journal of Microelectromechanical systems (2014)

Low velocity limit

$$Re_c = Gr^{1/3} \tag{13}$$

$$U_c = (g\alpha\nu\Delta T)^{1/3} \tag{14}$$

TSI 1201 wire in air	
α	$3.37 \times 10^{-3}\,\mathrm{K}^{-1}$
ν	$1.58 \times 10^{-5}\,\mathrm{m}^2/\mathrm{s}$
T_w	250 °C
T_∞	25 °C
U_c	4.9 cm/s

Chanal wire in cryogenic helium	
α	$5.77 \times 10^{-1}\,\mathrm{K}^{-1}$
ν	$7.77 \times 10^{-8}\,\mathrm{m}^2/\mathrm{s}$
T_w	15 K
T_∞	4.27 K
U_c	1.7 cm/s

Chanal, *et al.*, Eur. Phys. J. B **17**, 309-317 (2000)

Low velocity limit

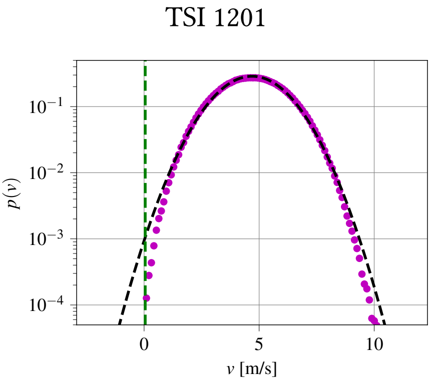

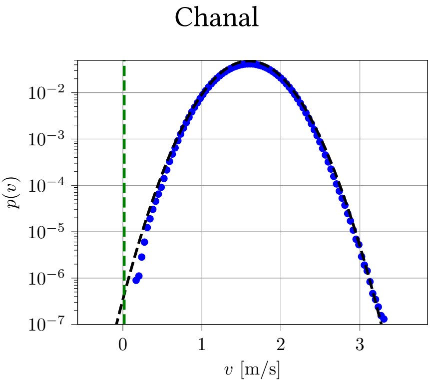

Chanal, *et al.*, Eur. Phys. J. B **17**, 309-317 (2000)

Hot wires

- No negative velocities
- Low velocity limit
- Fast and small.
- High frequency cutoff limited by CTA electronics
- Commercially available for room temperature
- Commercially available multi-sensor for multi-component measurements

REVIEW OF SCIENTIFIC INSTRUMENTS **76**, 075110 (2005)

Laser-cantilever anemometer: A new high-resolution sensor for air and liquid flows

Stephan Barth,[a)] Holger Koch, Achim Kittel, and Joachim Peinke
Carl von Ossietzky University of Oldenburg, D-26111 Oldenburg, Germany

Jörg Burgold and Helmut Wurmus
Center for Micro- and Nanotechnologies, D-98684 Ilmenau, Germany

(Received 10 December 2004; accepted 16 May 2005; published online 11 July 2005)

In this article, we present a technical description of a new type of anemometer for gas and especially liquid flows with high temporal and spatial resolution. The principle of the measurement is based on the atomic force microscope technique where microstructured cantilevers are used to detect extreme small forces. We demonstrate the working principle and the design of the sensor, as well as calibration measurements and initial measurements of turbulent flows, which were performed in air and water flows. © *2005 American Institute of Physics.* [DOI: 10.1063/1.1979467]

Principle

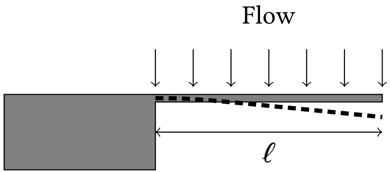

$$\frac{\Delta\ell}{\ell} \sim \frac{\mathrm{sign}(v)c_d(v)\rho v^2}{E}\frac{\ell^2}{e^2} \tag{15}$$

Barth, *et al.*, Rev. Sci. Instrum. **76**, 075110 (2005)
Salort, *et al.*, Rev. Sci. Instrum. **83**, 125002 (2012)
Salort, *et al.*, Rev. Sci. Instrum. **89**, 015005 (2018)

Straight cantilever

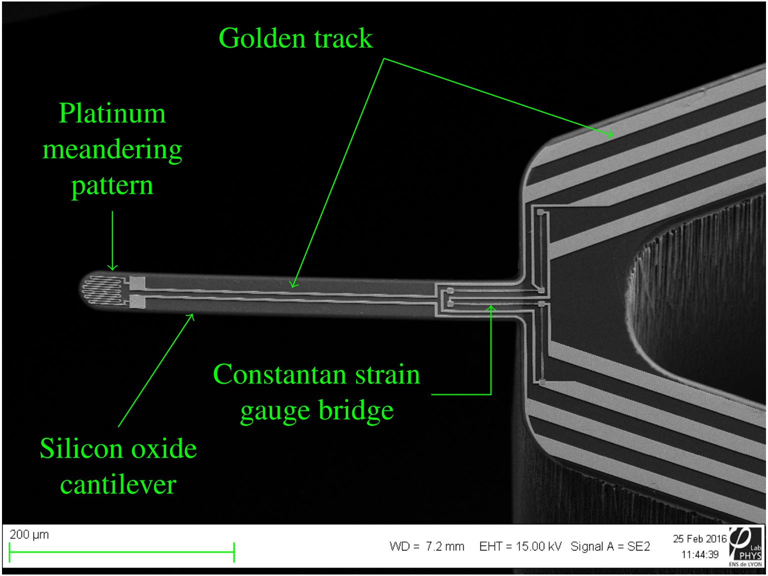

“Racket” cantilever

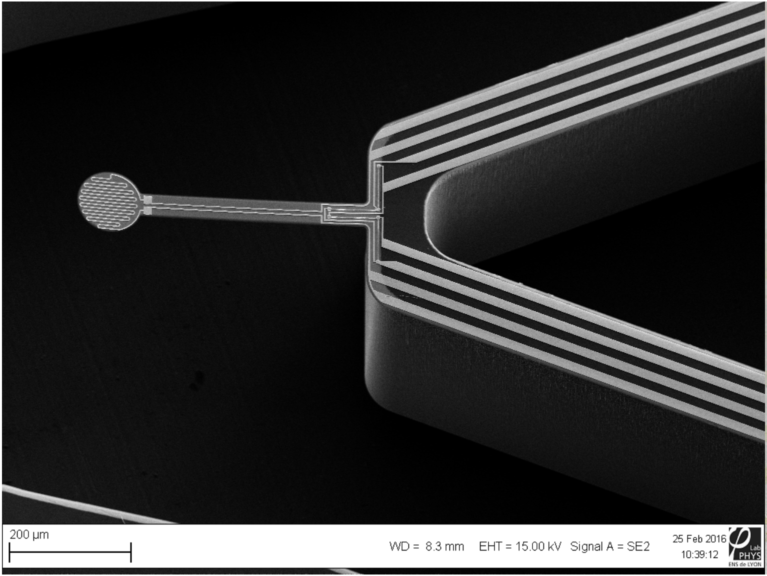

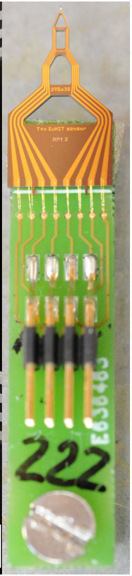

"Elongated" cantilever

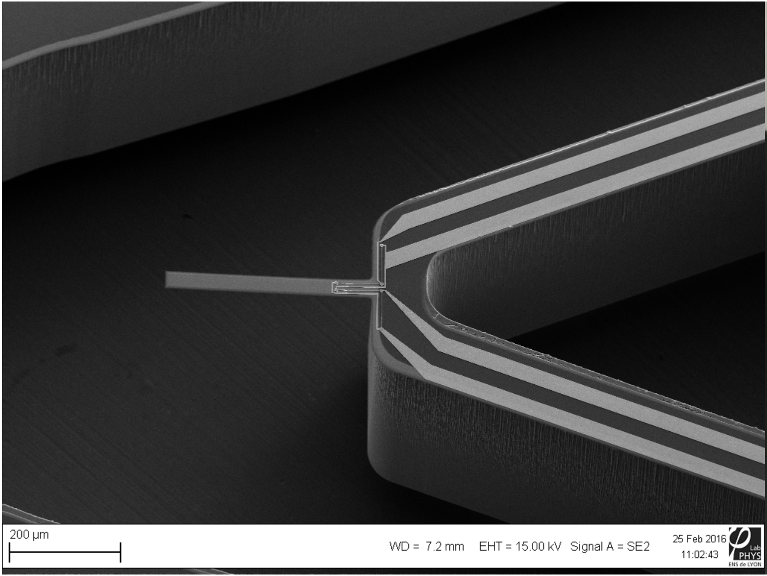

Sensor validation in air

- Potential cone: calibration *vs* hot-wire;
- Downstream: turbulent fluctuations.

Principle

Sensor validation in air: calibration law

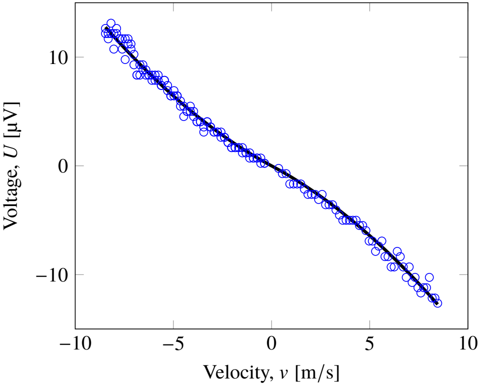

- Fit law:

$$U = av - \operatorname{sign}(v)\, bv^2$$

- Linear/Quadratic threshold:

$$v_0 = \left|\frac{a}{b}\right| \sim 15\,\mathrm{m/s}$$

$$Re_0 = \frac{wv_0}{\nu} = 34$$

Cantilever *vs* Hot-wire

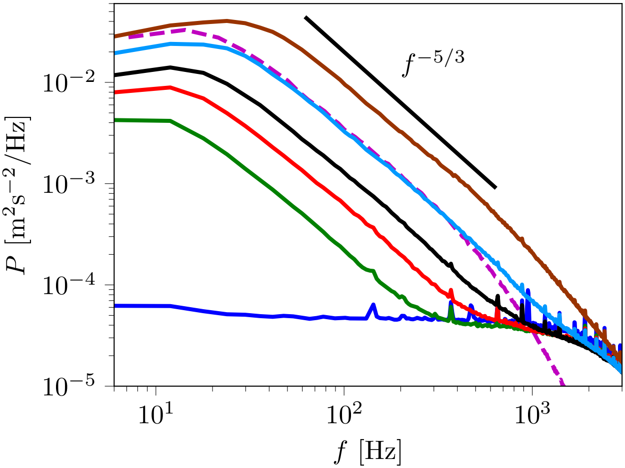

Cantilever *vs* Hot-wire

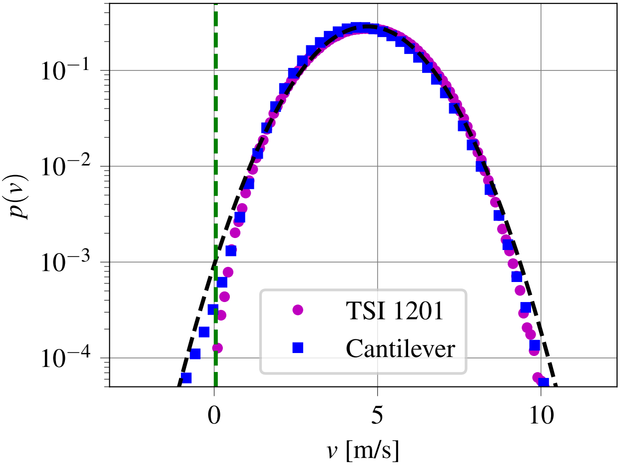

Low velocity limit caused by self-generated flow?

He I (3.1 K 1051 mbar)
110 μW

Frequency limitation: mechanical resonance

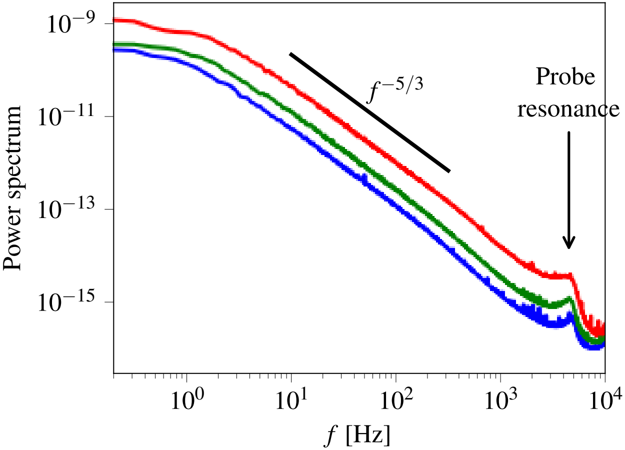

Data from GReC EuHIT Tritium experiment in gaseous helium
Collab. with P.-E. Roche, E. Rusaouën & B. Chabaud

Frequency limitations

$$f_{\mathrm{vac},n} = \frac{1}{2\pi} C_n^2 \frac{\theta}{\ell^2} \sqrt{\frac{E}{12\rho_c}} \tag{16}$$

where

$$1 + \cos C_n \cosh C_n = 0 \tag{17}$$

θ	cantilever thickness	1.2 µm
ℓ	cantilever length	300 µm
E	cantilever Young modulus	70 GPa
ρ_c	cantilever density	2200 $\mathrm{kg/m^3}$

$$f_1 = 7.8\,\mathrm{kHz}$$

Racket cantilever in vacuum

$$\frac{f_{\text{racket}}}{f_{\text{straight}}} = \left(1 + \frac{3\pi\Phi^2}{4\ell w}\right)^{-1/2} = 0.60 \tag{18}$$

Damping by the fluid

Inviscid model of Chu & Falconer (1963)

$$\frac{f_{\text{fluid}}}{f_{\text{vac}}} = \left(1 + \frac{\pi \rho_f w}{4\rho_c \theta}\right)^{-1/2} \tag{19}$$

when

$$Re_\omega = \frac{\pi f w^2}{2\nu} \gg 1 \tag{20}$$

Sader, J. Appl. Phys (1998)

Air	$Re_\omega \sim 1$
Water	$Re_\omega \sim 15$
Cryogenic gaseous helium	$Re_\omega \sim 100$

Frequency limitations

Typical values

- "Straight" in liquid helium: 5 kHz
- "Racket-shape" in liquid helium: 3 kHz
- "Racket-shape" in cryogenic helium gas: 4 kHz
- Shorter beam in vacuum ($\ell = 160\,\mu\text{m}$): 43 kHz

Cantilever anemometers

Advantages

- Signed velocity
- Linear in the low velocity limit
- Easier to operate in superfluid helium
- No spurious temperature signal

Drawbacks

- Low signal-to-noise ratio
- Mechanical resonance frequency

Outline

Eulerian point of view

- Variable: x. Fixed t. Parameter: ϵ.
- Kármán-Howarth equation:

$$S_p(\ell) = \langle (v(x+\ell) - v(x))^p \rangle_x (\ell) \tag{21}$$

$$S_3(\ell) = -\frac{4}{5}\epsilon\ell + 6\nu \frac{\mathrm{d}S_2(\ell)}{\mathrm{d}\ell} \tag{22}$$

- Kolmogorov spectrum:

$$P_{vv}(k) = C_k \epsilon^{2/3} k^{-5/3} \tag{23}$$

Sensor measurement

- Fixed position
- Fluctuations in time

$$v(t) \tag{24}$$

Frozen turbulence when $v_{rms} \ll v_{mean}$

Frozen turbulence when $v_{rms} \ll v_{mean}$

$$x = -\langle v \rangle t \rightarrow v(x) \tag{25}$$

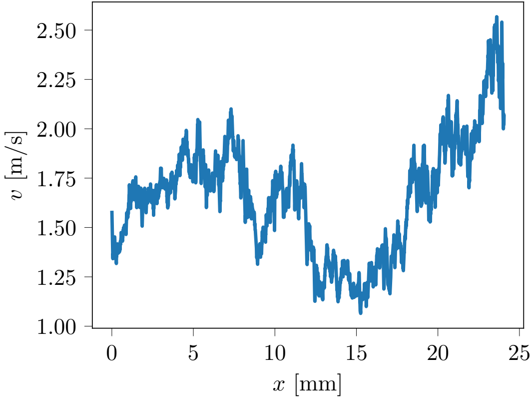

Chanal, *et al.*, Eur. Phys. J. B **17**, 309-317 (2000)

Higher turbulence intensity

- Turbulence intensity

$$\tau = \frac{v_{rms}}{v_{mean}} \tag{26}$$

- Chanal *et al.* round jet: $\tau = 23\,\%$
- Von Kármán flow (TSI hot-wire)

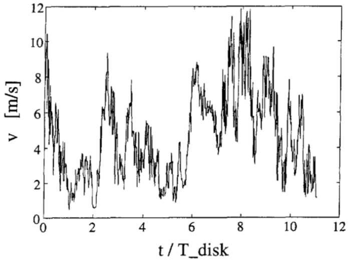

Fig. 2. — Measurement of velocity *vs.* nondimensional time $t/T_{\rm disk}$ where $T_{\rm disk}$ is the period of rotation of the disks.

Pinton & Labbé, J. Phys. II France **4**, 1461-1468 (1994)

Higher turbulence intensity

- Taylor hypothesis
  Spatial time series:

$$\left\{v(x_i) = v\left(t_i = x_i / \langle v \rangle\right)\right\}$$

- Local Taylor hypothesis

$$v(t) \;\rightarrow\; v(x), x = \int_0^t \bar{v}(\tau)\mathrm{d}\tau$$

$$\bar{v}(\tau) = \frac{1}{T}\int_{\tau-T/2}^{\tau+T/2} v(t)\mathrm{d}t$$

where T is the integral time scale.
$T = T_{disk}$ for Pinton & Labbé data.

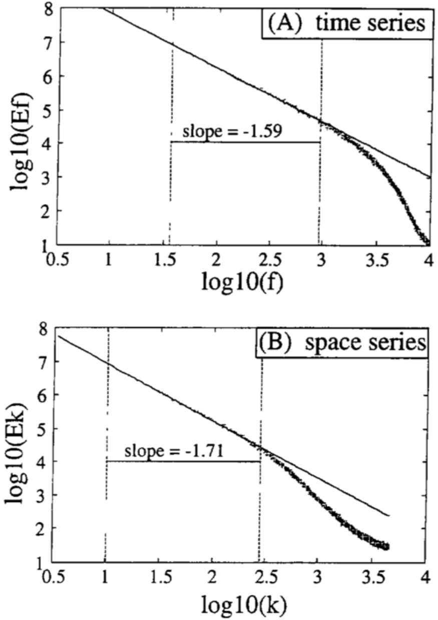

Fig. 4. — a): Power spectrum of time series. b): Power spectrum of resampled spatial series.

Moderate turbulence intensity

Chanal *et al.* ($\tau = 23\,\%$) used an Instantaneous Taylor hypothesis

$$x_i = \sum_{j<i} v_j \Delta t \tag{27}$$

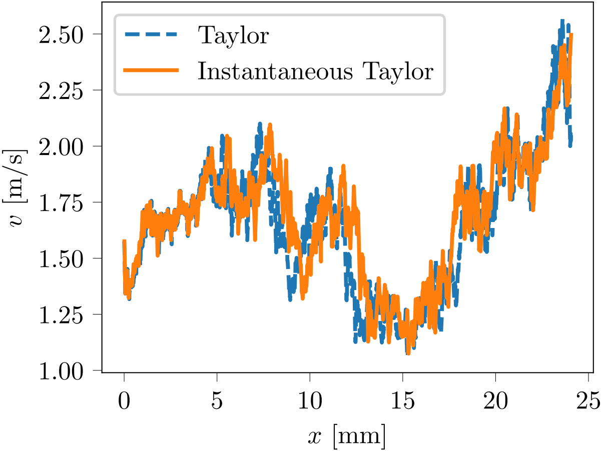

Instantaneous *vs* Local Taylor

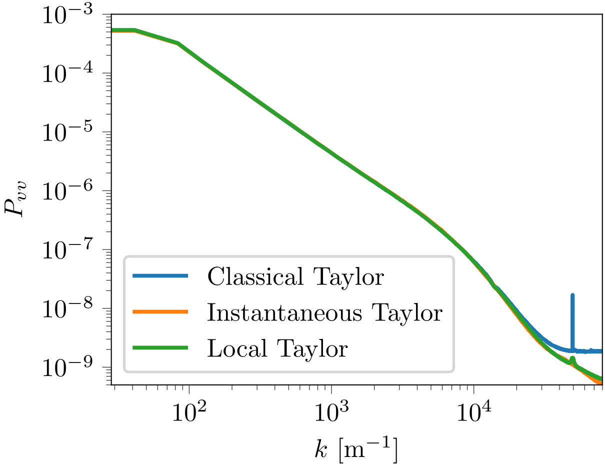

Local Taylor hypothesis for cantilever measurements

GReC EuHIT 2015 experiment (Tritium)
Collab. with P.-E. Roche, E. Rusaouën & B. Chabaud
$D_m = 48.5\,\mathrm{g/s}$

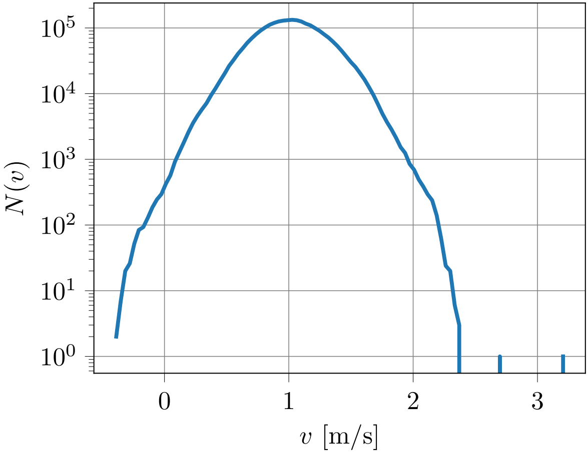

- There are $v_i < 0$.
- Instantaneous Taylor hypothesis does not make sense.
- Local Taylor hypothesis is OK.

Local Taylor hypothesis for cantilever measurements

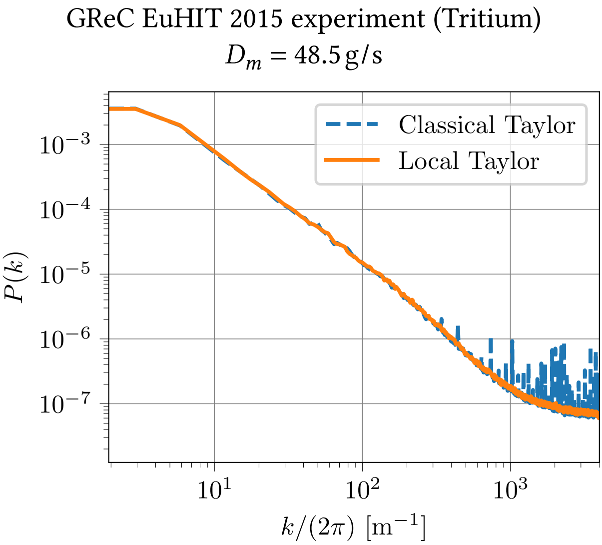

Taylor hypothesis

- Classical Taylor hypothesis fine for low turbulence intensity;
- Local Taylor hypothesis (Pinton & Labbé) necessary for larger turbulence intensity;
- Instantaneous Taylor hypothesis (Chanal) does not make sense for signed velocity
- Resampled signal hides spurious EM peaks

He & Zhang, PRE (2006)

- Space-time correlation function

$$C_v(z,\tau) = \frac{\langle u(x+z,t+\tau)u(x,t)\rangle}{\sigma^2} \tag{28}$$

- One sensor: $C_v(0,\tau)$.
- Desired quantity: $C_v(r,0)$ ($\rightarrow$ power spectrum density)
- Taylor frozen turbulence hypothesis:

$$C_v(r,\tau) = C_v(r-U\tau,0) \tag{29}$$

He & Zhang, PRE (2006)

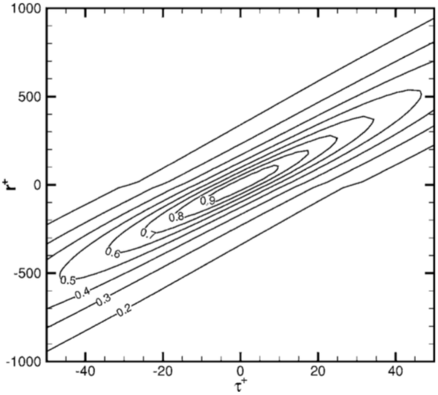

FIG. 1. Contours of space-time correlations $R(r,\tau;x_2^+)$ at $x_2^+ = 12$ as a function of space and time separations.

Elliptic approximation (EA) model

$$C_v(r,\tau) = C_v(r_c, 0), \tag{30}$$

with

$$r_c^2 = (r - U\tau)^2 + V^2\tau^2. \tag{31}$$

$$U = \langle u(t) \rangle, \tag{32}$$

$$V = \langle (u(t) - U)^2 \rangle^{1/2} \tag{33}$$

For $V = 0$, Taylor hypothesis is recovered.

Extension to temperature correlation

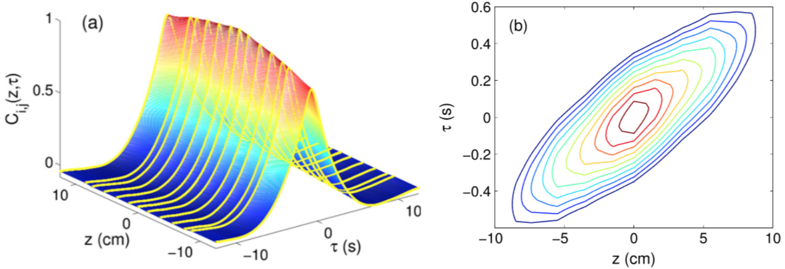

Figure 9. (a) A three-dimensional rendering of the experimental results for the cross-correlation function $C_{i,j}(z,\ \tau)$. (b) Experimental constant-correlation contours of $C_{i,j}(z,\ \tau)$ in the z-τ plane. All measurements are for $Ra = 1.25 \times 10^{14}$, $Pr = 0.86$.

He, *et al*, New J. Phys. **17**, 063028 (2015)

Application to velocity measurement in thermal flows

- Two thermometers separated by d
  Autocorrelation yields $C_{11}(\tau) = C(0,\tau)$
  Intercorrelation yields $C_{12}(\tau) = C(d,\tau)$
- Find τ_d such as
  $$C_{11}(\tau_d) = C_{12}(0)$$
  i.e.
  $$C(0,\tau_d) = C(d,0)$$
- Find τ_p where C_{12} is maximum
- EA yields
  $$\alpha_0 = \tau_d/d$$
  $$\alpha_p = \tau_p/d$$
  $$U = \alpha_p/\alpha_0^2$$
  $$V = \sqrt{1-(\alpha_p/\alpha_0)^2}/\alpha_0$$

Application to velocity measurement in thermal flows

Chavanne Rayleigh-Bénard cell. 20 cm-high. Gaseous helium.
200 µm cubic thermometers, 2.3 mm apart

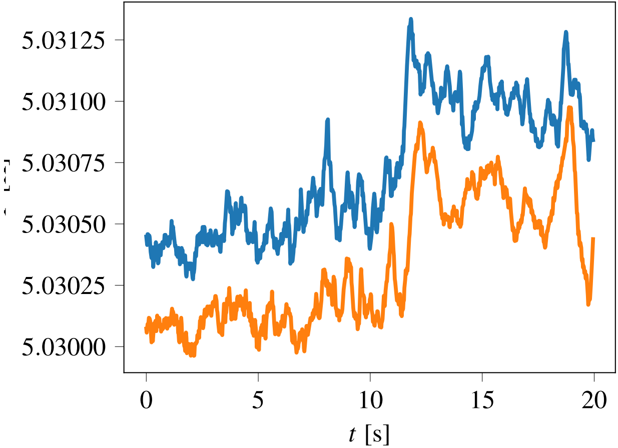

Chavanne, *et al*, Phys. Fluids (2001)

Application to velocity measurement in thermal flows

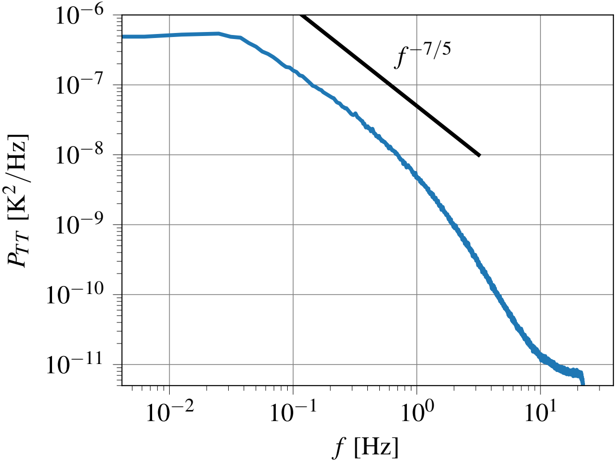

Chavanne, *et al*, Phys. Fluids (2001)

Side note on small scale properties of temperature

Parameters

- Kinetic energy dissipation rate

$$\epsilon = \frac{\nu}{2} \sum_{i,j} \left(\frac{\partial u_i}{\partial x_j} + \frac{\partial u_j}{\partial x_i} \right)^2 \tag{34}$$

- Thermal dissipation rate

$$\epsilon_\theta = \kappa \sum_{i} \left(\frac{\partial T}{\partial x_i} \right)^2 \tag{35}$$

Side note on small scale properties of temperature

$$[\epsilon] = \mathrm{m}^2/\mathrm{s}^3 \tag{36}$$

$$\left[\epsilon_\theta\right] = \mathrm{K}^2/\mathrm{s} \tag{37}$$

ϵ is the governing parameter

$$\langle \delta v^2 \rangle \sim (\epsilon r)^{2/3} \tag{38}$$

$$\langle \delta T^2 \rangle \sim \epsilon_\theta \epsilon^{-1/3} r^{2/3} \tag{39}$$

Obukhov (1949) and Corrsin (1951)

Side note on small scale properties of temperature

$$[\epsilon] = \mathrm{m}^2/\mathrm{s}^3 \tag{40}$$

$$[\epsilon_\theta] = \mathrm{K}^2/\mathrm{s} \tag{41}$$

$$[\alpha g] = \mathrm{ms}^{-2}\mathrm{K}^{-1} \tag{42}$$

ϵ_θ and αg are the governing parameters

$$\langle \delta v^2 \rangle \sim \epsilon_\theta^{2/5} (\alpha g)^{4/5} r^{6/5} \tag{43}$$

$$\langle \delta T^2 \rangle \sim \epsilon_\theta^{4/5} (\alpha g)^{-2/5} r^{2/5} \tag{44}$$

Bolgiano (1959)

Crossover scale: Bolgiano scale

$$L_B = \epsilon^{5/4} \epsilon_\theta^{-3/4} (\alpha g)^{-3/2} \tag{45}$$

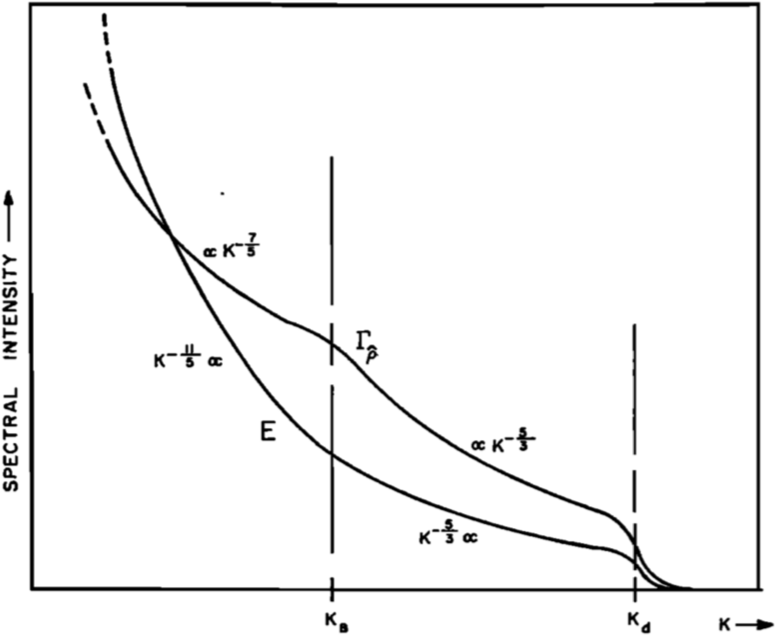

FIG. 1—Spectral forms in a stably stratified atmosphere.

Application to velocity measurement in thermal flows

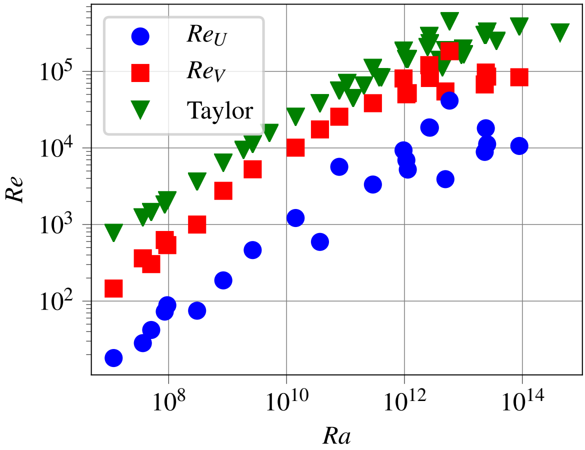

EA on Chavanne data

- $Re_U \ll Re_V < Re_{\text{Taylor}}$
- Re_U statistical convergence less good
- Why?

Local Elliptic Approximation

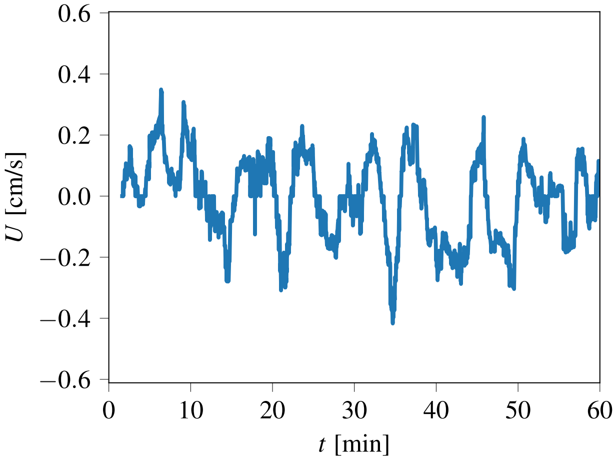

Comparison with the original Chavanne *et al* method

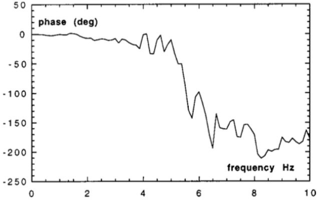

FIG. 9. Phase of the cross correlation spectrum vs the frequency for the session Pr=1.3, Ra=1.35×10^{12}, ΔT=103 mK.

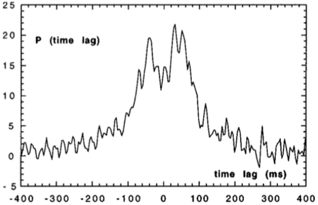

FIG. 10. Time lag distribution for Pr=1.3, Ra=1.35×10^{12}, ΔT=103 mK, performed through reverse Fourier transform. Note that positive and negative time lags have essentially the same probabilities.

Outline

Examples of local probes
- Hot wire (CTA)
- Cantilever anemometers

Frozen turbulence
- Local Taylor hypothesis
- Elliptic approximation

Experimental characterisation of turbulence
- Longitudinal velocity increments
- Application: energy cascade in superfluid flows
- Extended Self-similarity
- Application: intermittency of superfluid flows

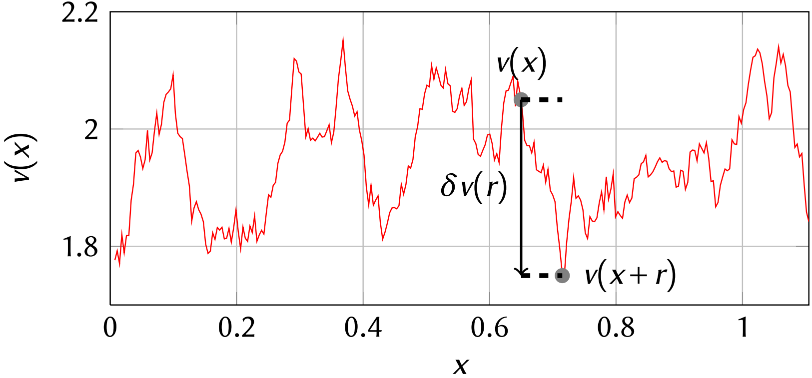

2.2
2
1.8
0
0.2
0.4
0.6
0.8
1
x
$v(x)$
$v(x)$
$\delta v(r)$
$v(x+r)$

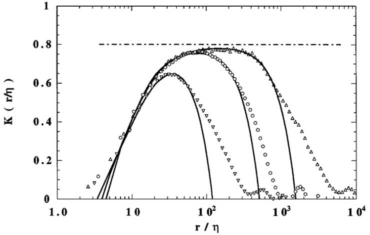

FIG. 2. The Kolmogorov function $K(r) = -S_3/\epsilon r$ versus r/η, for different Reynolds number R_λ. The values of ϵ are obtained by using best fits, as discussed in the text. (▽): $R_\lambda = 120$; (○): $R_\lambda = 300$; (△): $R_\lambda = 1170$. The solid lines show the expected curves, obtained from Eq. (1).

Moisy, *et al.*, Phys. Rev. Lett. (1999)

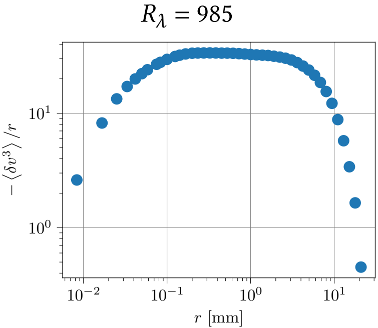

Chanal, *et al.*, EPJB (2000)

Results from SHREK 2017

- Racket-shape cantilever, $\ell = 375\,\mu\mathrm{m}$
- 40 mm from the lateral wall
- Cell mid-height

Results from SHREK 2017

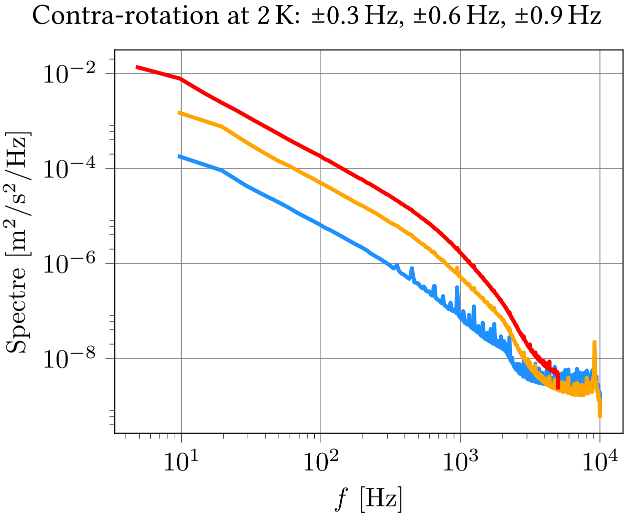

Results from SHREK 2017

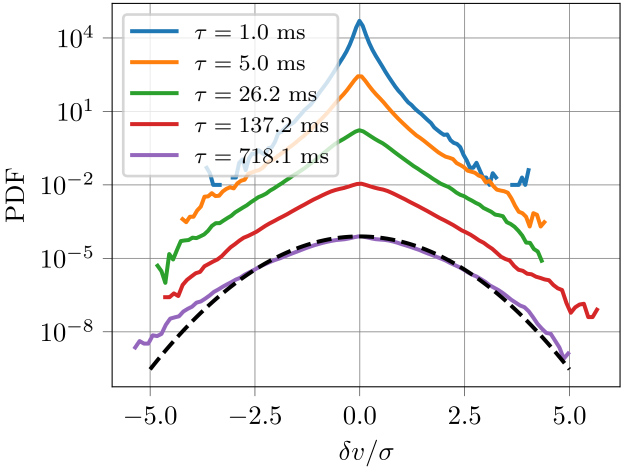

Local Taylor hypothesis

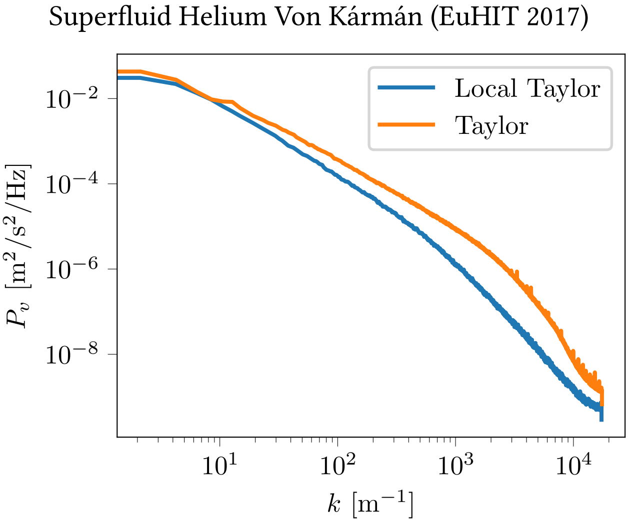

Local Taylor hypothesis

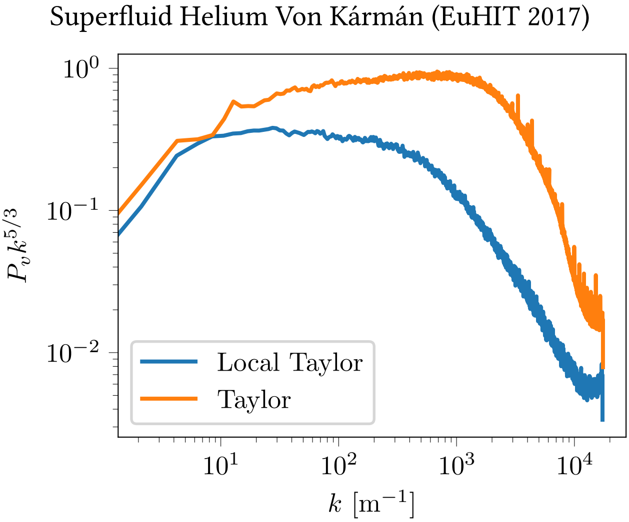

Evidence of kinetic energy cascade

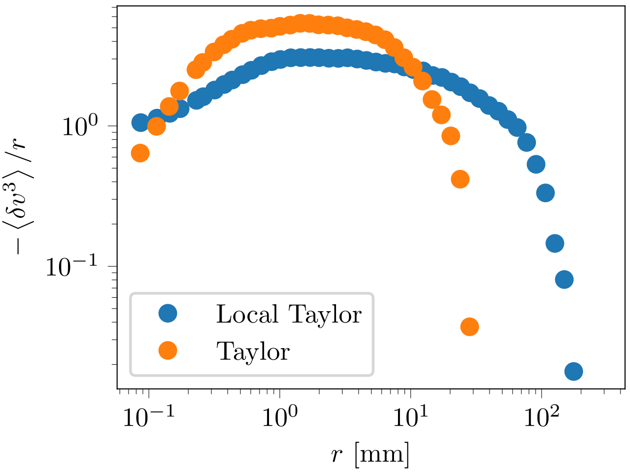

Characterization of deviation from K41

$$\langle (\delta v)^p \rangle \propto (\epsilon \ell)^{\zeta_p} \tag{46}$$

For K41,

$$\zeta_p = \frac{p}{3} \tag{47}$$

Experimental problem

- Odd values of p do not converge well
- Large values of p do not converge well
- Experimental determination of ζ_p difficult

Extended self-similarity

$$\langle|\delta v(\ell)|^p\rangle \propto \langle|\delta v(\ell)|^3\rangle^{\zeta_p} \tag{48}$$

$$\left|\langle\delta v(\ell)^3\rangle\right| \approx \langle|\delta v(\ell)|^3\rangle \tag{49}$$

ESS on Chanal data

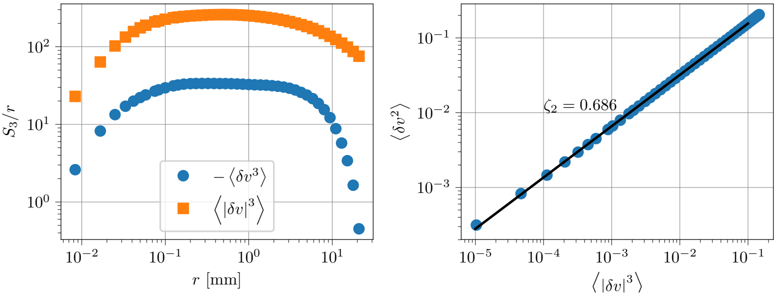

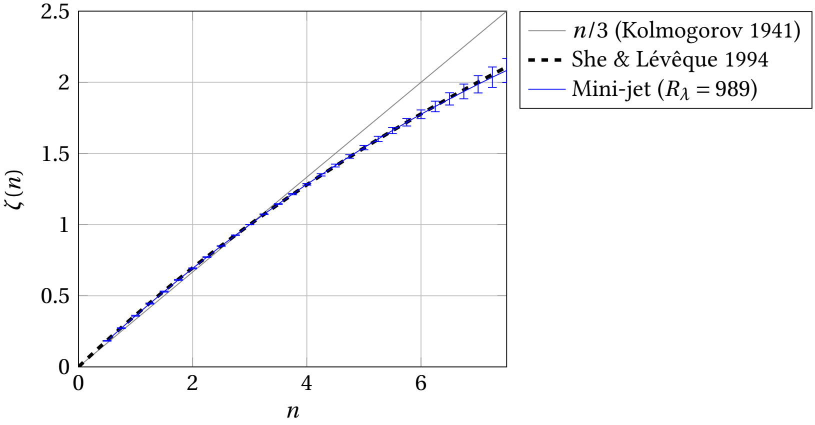

2.5
2
1.5
1
0.5
0
0
2
4
6
$\zeta(n)$
n
$n/3$ (Kolmogorov 1941)
She & Lévêque 1994
Mini-jet ($R_\lambda = 989$)

Application to intermittency of superfluid flows

TABLE I. Experimental and numerical studies of quantum turbulence intermittency. The statements "more" or "less" intermittent are based on structure functions of order larger than two (e.g., as shown in Fig. 11). The second order structure function can suggest an opposite trend.

References	Approach	Superfluid fraction ρ_s/ρ (%)	Intermittency exponents ($\zeta_{p\geqslant 3}$)
Maurer and Tabeling[10]	Experiment	92	Consistent with classical
Salort *et al.*[11]	Experiment	0 and 85	Consistent with classical
	DNSs (based on HVBK)	9 and 98	Consistent with classical
Boué *et al.*[12]	Shell-model simulations	~20 – 90	*More intermittent*
	(Based on HVBK)	$\lesssim$20 or $\gtrsim$90	Consistent with classical
Shukla and Pandit[14]	Shell-model simulations	~10 – 80	*Less intermittent*
	(Based on HVBK)	$\lesssim$40 or $\gtrsim$65	Consistent with classical
Bakhtaoui and Merahi[15]	LES simulations	84	*More intermittent*
	(Based on HVBK)	23 and 98	Consistent with classical
Krstulovic[16]	Gross-Pitaevskii simulation	100	*More intermittent*
Rusaouen *et al.*[17]	Experiment	0, 19, and 81	Consistent with classical
Rusaouen *et al.* (present study)	Experiment	0, 11.3, 51, 63, 85.8, and 95.7	Consistent with classical

Rusaouën, *et al*, Phys. Fluids (2017)

Cantilever anemometer in the Toupie wind tunnel

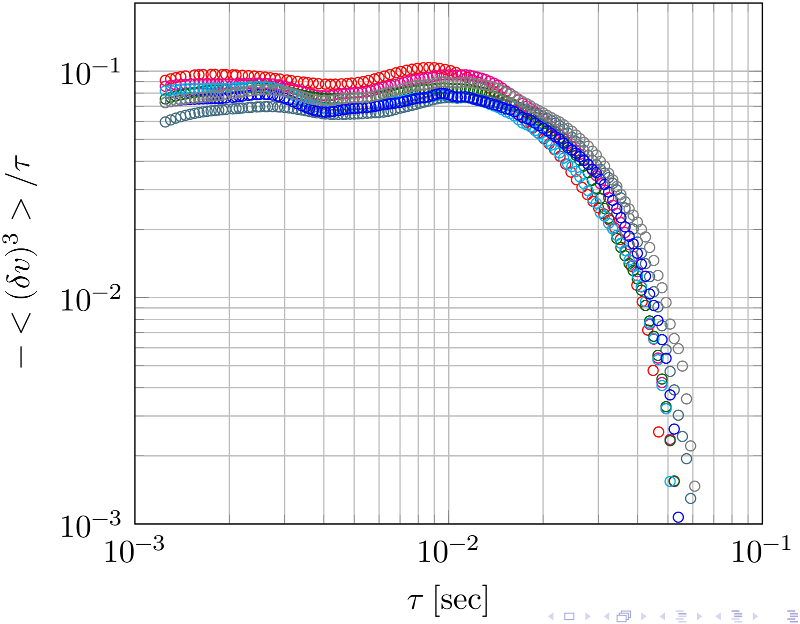

ESS on cantilever data in superfluid Toupie

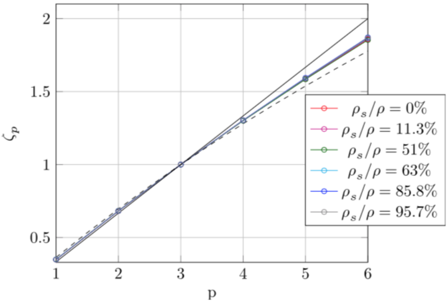

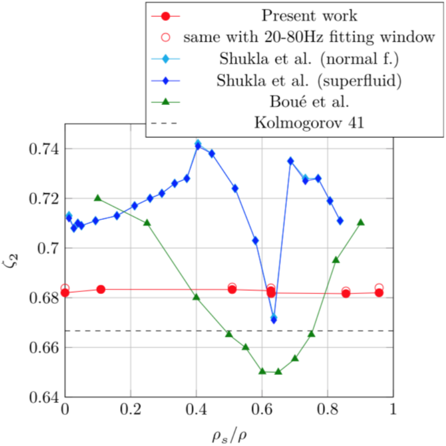

Conclusions

Local investigation of velocity fluctuations

- Hot-wire small and fast but not suited to all situations
- Cantilever well suited to superfluid flows and Von Kármán flows
- Extension of Taylor hypothesis necessary in VK and RBC
- ESS: useful tool for ζ_p